Peptide-mediated surface-immobilized quantum dot hybrid nanoassemblies with controlled photoluminescence†‡

Melvin T. Zin,[a] Andrea M. Munro,[b] Mustafa Gungormus,[a] Ngo-Yin Wong,[a] Hong Ma,[a] Candan Tamerler,[c] David S. Ginger,[b] Mehmet Sarikaya[a] and Alex K.-Y. Jen*[ab]

Received 16th October 2006, Accepted 21st November 2006
First published as an Advance Article on the web 7th December 2006
DOI: 10.1039/b615010a

Combinatorially selected peptides and peptide–organic conjugates were used as linkers with controlled structural and organizational conformations to attach quantum dots (QDs) at addressable distances from a metal surface. This study demonstrates an approach towards nanophotonics by integrating inorganic, organic, and biological constructs to form hybrid nanoassemblies through template-directed self-assembly. Peptide–organic-linked QD arrays showed stronger fluorescence than peptide-linked QD arrays. We attribute this difference primarily to the increased number density of QDs on peptide–organic-linked QD arrays.

Introduction

Peptide-mediated assembly of inorganic nanomaterials offers a powerful approach to form hybrid nanostructures.[1] Apart from their self-assembly and molecular recognition for inorganic surfaces, designed peptides are robust and can be genetically engineered to tailor their functionalities such as binding, linking, erecting, and bracing.[2] In addition to twenty commonly occurring amino acids, there are variants and synthetic analogues available to produce a virtually unlimited variety of peptides and polypeptides.[3] Furthermore, functional groups (*e.g.*, carboxyls and amines) appended to the amino acids can be exploited for different chemical reactions.[4] Similarly, metallic and semiconductor nanomaterials with desired electrical, optical, or magnetic properties can be synthesized for intended applications in electronics, optoelectronics, or sensing by controlling their size, shape, composition, and surface chemistry.[5] By combining the conformational advantages of peptides with the useful attributes of nanomaterials, peptide–inorganic hybrid nanoassemblies can potentially be endowed with tunable properties for a wide range of applications in nanobiotechnology.[6]

In recent years, hybrid nanostructures composed of core–shell quantum dots (QDs) and proteins have become a subject of considerable interest for developing novel sensors and biomaterials.[7–10] For example, maltose-binding protein conjugated to CdSe–ZnS QDs were used as probes in immunoassays and as active components in sensors based on Förster resonance energy transfer.[8] In a separate approach, peptides were directly immobilized onto the surface of QDs to improve their stability in aqueous media and to greatly enhance their biocompatibility.[9] In addition, the versatility of proteins has been exploited in the assembly of QDs to form hybrid nanostructures in solution.[10] While much work has been accomplished in solution, less effort has been invested in the construction of protein–QD hybrid nanoassemblies on solid supports.[11] Surface immobilization of QDs at specific sites in arrays constitutes an essential step towards fabricating devices, and is necessary for fundamental understanding of electronic and optical interactions within the ensembles of QDs.[12] Although there have been spectral studies on surface-bound QDs,[13] spectral characterizations on arrays of protein–QD hybrid nanoassemblies have not yet been carried out. Therefore, investigations towards revealing the effects of the geometrical arrangement of QD ensembles with high solid-state packing densities and the populations of QDs within these ensembles on absorption, scattering, and luminescence properties of hybrid nanostructures are lacking.

We report here the utility of genetically engineered peptides as biomolecular linkers to direct the self-assembly of QDs into periodic arrays on a metal surface and the use of spatially resolved spectral measurements of fluorescence from the resulting hybrid nanostructures. This study is the first step towards investigating surface-plasmon-enhanced luminescence properties of peptide–QD hybrid nanoassemblies for optoelectronic and sensing applications through control of the QD–metal distance using peptide linkers. Conventional approaches to assemble QDs have been based on thiol or silane linkages, hydrogen bonding, Coulombic attraction, and van der Waals forces.[14] These interactions, however, are non-specific toward a given substrate; for example, thiols will bind indiscriminately to any metal—gold, silver, or platinum. Our approach is unique in the application of combinatorially selected peptides as linkers. Using peptides to exquisitely control the range of physical properties and ordering of inorganic nanomaterials is one of the major promises of

[a]*Department of Materials Science and Engineering, University of Washington, Seattle, Washington, USA. E-mail: ajen@u.washington.edu; Fax: (+1) 206-543-3100; Tel: (+1) 206-543-2626*
[b]*Department of Chemistry, University of Washington, Seattle, Washington, USA*
[c]*Department of Molecular Biology and Genetics, Istanbul Technical University, Istanbul, Turkey*

† Electronic supplementary information (ESI) available: experimental details on materials, substrate preparation, patterning, self-assembly, AFM characterization, fluorescence microscopy, and spatially resolved fluorescence spectroscopy. See DOI: 10.1039/b615010a

‡ The HTML version of this article has been enhanced with colour images.

molecular biomimetics.[2] Employing both phage display and cell surface display technologies, we have developed genetically engineered peptides for inorganics (GEPIs)[15] with surface recognition for metals[16–18] and metal oxides.[19] In this study, gold-binding peptide (GBP1) was used as a model.[17,18] In comparison to self-assembled monolayers (SAMs) or electrostatically charged polymers that are commonly used as linkers for QD attachment,[13,14] the unparalleled benefit of GEPIs is their potential ability to recognize elemental composition, crystallographic structure and orientation, and morphology of an inorganic surface.[15,16,20,21] We demonstrate the potential of using GEPIs to systematically vary the distance of QDs from a metal surface and to tailor their spatial configurations within the patterned ensembles in surface-plasmon-coupled fluorescence studies. By exploiting reactive groups appended to the amino acids, we show that, as biomolecular linkers, GEPIs can be covalently bonded with π-conjugated functional molecules through surface chemical reaction to manipulate their structural organization, which in turn regulates their biological functionality. We observe an increase in the average QD attachment density when peptide–organic conjugates are employed in the formation of hybrid nanostructures, producing periodic arrays with controlled photoluminescence through a combination of tunable QD number density and well-defined QD–metal spacing.

Results and discussion

The 14-amino-acid-long GBP1 (MHGKTQATSGTIQS), combinatorially selected and further engineered, exhibits an interesting dual trait. It binds to gold surfaces and controls morphogenesis of gold nanoparticles that predominantly feature {111} crystallographic surfaces.[15,17] Interestingly, GBP1 does not include cysteine or histidine, two residues known to bind with metals.[17] Experimental and modeling studies have shown an increase in the binding strength of GBP1 on the gold surface with 3-repeats compared to 1-repeat.[18] In this work, as an additional functionality, we incorporated biotin (bio) to 3-repeat GBP1 (bio-3RGBP1, bio-[MHGKTQATSGTIQS]$_3$) at the N-terminus to create a bifunctional construct which serves as a binder for specific adsorption to the gold substrate as well as a receptor for controlling the self-assembly of streptavidin (SA) functionalized CdSe–ZnS QDs (SA-QDs) through bio-SA binding. We chose to use bio-SA binding for the following reasons: (i) it is one of the strongest ligand–receptor interactions found in nature (dissociation constant: $K_d \sim 10^{-15}$ M); (ii) its bond formation is well understood; (iii) the reaction between bio and SA is relatively fast (within ~30 min); and (iv) the resulting bio-SA complexes are extremely stable over a wide range of temperature and pH.[22] Each SA-QD ranges in diameter from 15 nm to 18 nm and contains 5 to 10 SA molecules covalently attached onto the surface of a QD through ester formation.[23] Their emission spectrum is narrow and symmetric (full width at half maximum, FWHM, ~30 nm) with the peak maximum near 605 nm.[23]

Incorporating QDs into devices for many applications, such as array-based chemical and biological sensors, requires governing their self-assembly characteristics and their positional arrangement on solid supports.[12] To achieve spatial control over the peptide-mediated formation of QD hybrid nanoassemblies, gold substrates patterned by microcontact printing (μCP)[24] were used as templates (Fig. 1). We employed μCP for its experimental simplicity and its capability to generate patterns over a centimeter-scale area in a parallel fashion. As illustrated in Fig. 1, two schemes were formulated to vary the spacing between QDs and gold surface (determined by the linker length) and to examine the functionality of

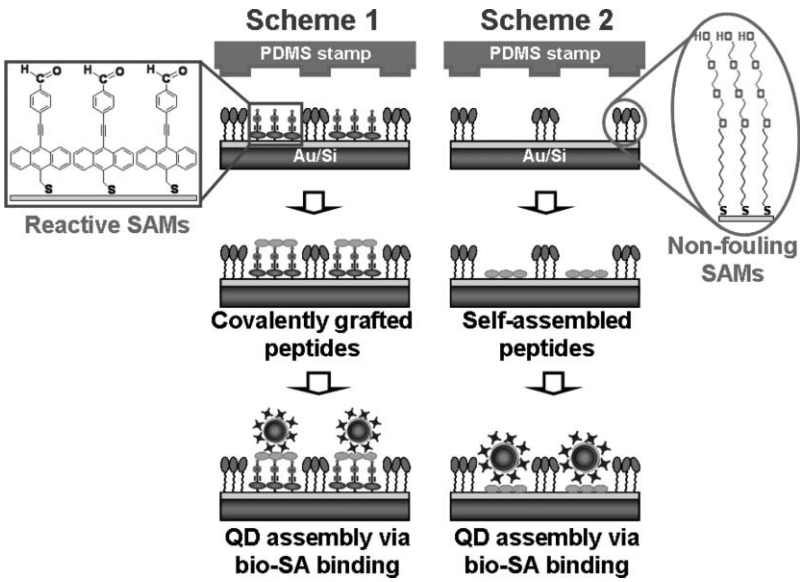

Fig. 1 Sketch of the experimental procedure. A gold substrate patterned by μCP of OEG provides a template to allow the sequential self-assembly of linkers and QDs in a site-specific fashion into periodic arrays. In Scheme 1, the patterned gold substrate was backfilled with MMAPA, followed by the covalent attachment of peptides onto MMAPA through Schiff base formation between $-NH_2$ groups on peptides and –CHO end-groups of MMAPA. In Scheme 2, peptide linkers were directly immobilized onto the gold substrate through surface recognition. Because of the difference in heights of peptide linkers and MMAPA-grafted peptide linkers, QDs are attached at different distances from the metal surface.

bio-3RGBP1 when covalently bonded with π-conjugated functional molecules. Since the biological functionality of peptides is mainly related to their structural conformation, covalent attachment of bio-3RGBP1 onto the SAMs of fused-ring aromatic thiols is anticipated to alter their physical characteristics and, therefore, their binding behavior and molecular recognition.

Achieving highly selective placement of QDs is essential on the substrate while minimizing non-specific interactions during self-assembly for producing devices where the patterned formation of hybrid nanostructures is required. Therefore, both schemes described in Fig. 1 begin with the patterning of gold substrates ($\sim$1 cm^2) by μCP of 11-mercaptoundecyl-tri(ethylene glycol)alcohol (OEG; 1 mM ethanolic solution) that serves as a non-fouling coating. Within areas where the polydimethylsiloxane stamp is in contact with the gold substrate, SAMs of OEG are formed within $\sim$20 s while non-contact areas remain unmodified. The regions passivated with OEG effectively resist adsorption of proteins.[25] As a result, layer-by-layer self-assembly of bio-3RGBP1 and SA-QDs was achieved in a site-specific manner onto the regions unmodified by the printed OEG SAM.

We have capitalized on the surface chemical reaction to covalently bond bio-3RGBP1 onto the SAM of fused-ring aromatic thiols. Covalent attachment of peptides is a critical issue in the development of diagnostic assays and drug discovery platforms.[26] This process is facilitated by a simple means of anchoring peptides onto pre-formed SAMs with selective and efficient reactivity. As outlined in Scheme 1 of Fig. 1, the patterned gold substrate is immersed into a degassed solution of (10-mercaptomethyl-9-anthryl)(4-aldehydephenyl)acetylene (MMAPA; 0.5 mM ethanolic solution) to produce reactive sites for covalent attachment of bio-3RGBP1 through Schiff base formation (–HC=N–) between amine groups (–NH_2) on bio-3RGBP1 and aldehyde end-groups (–CHO) on MMAPA. Typically, covalent attachment of peptides is carried out on SAMs with carboxylic (–COOH) functionality in a two-step procedure that involves the formation of interchain carboxylic anhydride as an intermediary.[27] In contrast, Schiff base formation is a one-step procedure that occurs under ambient conditions and produces water as the only by-product.[28] In addition, SAMs of MMAPA may be used to anchor not only peptides[29] but also non-biological organic compounds with amine functionality.[30] Unique features of MMAPA are the way in which the –CHO terminal group is exposed at the terminus of its ethynylphenyl moiety to promote surface chemical reaction with minimal steric hindrance and the presence of the anthracene moiety that allows parallel-displaced π–π stacking with its neighboring molecules to yield densely packed and highly organized SAMs.[29,30] Noticeably, MMAPA possesses a sturdy framework to resist conformational instability that would inevitably be induced by the formation of layered architectures involving additional phases.[29,30] After the backfilling by MMAPA, the sample was copiously rinsed with ethanol and chloroform.

As the second step in both schemes, immobilization of peptides is carried out by incubating the samples in a solution of bio-3RGBP1 (5 μg mL^{-1}) in phosphate-buffered saline (PBS, pH 7.4) for 90 min and 30 min for Scheme 1 and Scheme 2, respectively. In Scheme 2, specific adsorption of bio-3RGBP1 occurs through surface recognition. In Scheme 1, covalent attachment of bio-3RGBP1 takes place through surface chemical reaction. Each unit (*i.e.*, three repeats) of bio-3RGBP1 contains three –NH_2 groups appended to the lysine residues for potential coupling with the –CHO end-groups of MMAPA. In both cases, the non-fouling property of the OEG SAM ensures the immobilization of bio-3RGBP1 in a site-specific fashion. Prior to the assembly of QDs in the final step, the samples were thoroughly rinsed in PBS to remove excess bio-3RGBP1 on the surface, followed by deionized water to remove any salt residue from PBS. After incubating the samples in a SA-QD solution for 45 min to allow the bio-SA binding to complete, unbound QDs were washed off with PBS and deionized water.

The peptide-mediated sequential self-assembly process can be visualized by atomic force microscopy (AFM) as displayed in Fig. 2 for the formation of hybrid nanostructures composed of MMAPA, bio-3RGBP1, and SA-QDs (Scheme 1 in Fig. 1).

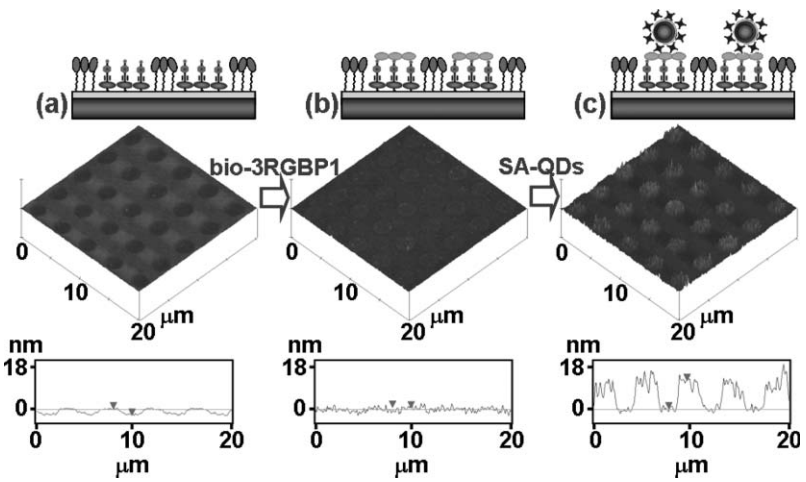

Fig. 2 Template-directed sequential self-assembly of MMAPA, bio-3RGBP1, and SA-QDs into periodic arrays of 2 μm circles (Fig. 1, Scheme 1). Formation of QD hybrid nanoassemblies showed the specificity of layer-by-layer assembly and spatial organization.

For AFM studies, arrays of 2 μm holes (*i.e.*, areas unmodified by the printed OEG SAM) were used as a template. After backfilling MMAPA into the holes, cross-sectional analysis revealed that the areas passivated by OEG were ~1.6 nm taller (Fig. 2a ↔ Fig. 1, Scheme 1, step 1). This is in agreement with the thickness difference between the SAMs of OEG (2.9 ± 0.3 nm)[25] and MMAPA (1.3 ± 0.2 nm).[29,30] In the next step, covalent bonding of bio-3RGBP1 onto the SAMs of MMAPA led to another height increase of ~1.5 nm and the leveling of surface topography (Fig. 2b ↔ Fig. 1, Scheme 1, step 2), corresponding to the immobilization of a layer of bio-3RGBP1. Negligible non-specific adsorption of peptides onto the non-reactive areas of the arrays was observed. A dramatic change of surface topography resulted with the assembly of SA-QDs (Fig. 2c ↔ Fig. 1, Scheme 1, step 3). A height increase of about ~15–18 nm in the cross-sectional profile confirmed the QD attachment.

To investigate the dependence of the luminescence properties of peptide–QD hybrid nanoassemblies on linker length as well as the ordering and number density of QDs within the arrays, fluorescence microscopy and spectroscopy were performed. Arrays of 10 μm lines were used to obtain long-range correlation in the average QD attachment density. For qualitative comparison of emission intensities from QD arrays, fluorescence images were taken on an inverted Nikon microscope (Eclipse TE2000-U) equipped with a tungsten halogen lamp as an excitation source. Fig. 3a and c show that, as expected, most PL comes from the regions where the QDs were specifically attached. There is a strong contrast in PL between the hybrid nanostructures and the OEG-passivated regions, demonstrating precise alignment of the arrays, good reproducibility, and uniformity of the template-directed self-assembly process over large areas.

The emission intensity of a fluorophore immobilized on a metal surface depends on the competition between physicochemical processes that can potentially both enhance and quench the fluorescence.[31] This interplay is particularly sensitive to the distance between fluorophore and metal. For flat metal surfaces, we expect quenching to dominate enhancement, and the fluorophores closer to the metal are expected to be quenched more severely than those spaced farther away.[32] On this basis, since the distance between QDs and gold substrate is ~8.65 nm when bio-3RGBP1 linkers are used and ~9.95 nm when MMAPA-grafted bio-3RGBP1 linkers are used (see ESI† for details), one might expect to see more fluorescence from MMAPA–peptide-linked QD arrays. Indeed, the analysis of fluorescence images proved this hypothesis. The emission intensity from arrays of hybrid nanostructures with MMAPA (Fig. 3c) was stronger than that from arrays of hybrid nanostructures without MMAPA (Fig. 3a). In a control experiment, when SA-QDs were physisorbed onto the gold substrate, PL was weak with a low signal-to-background ratio since their separation from the gold substrate was reduced to ~5 nm or less.

However, in addition to affecting the QD–metal spacing, MMAPA–peptide linkers also alter the average QD attachment density. Between the two types of attachment chemistry, the differences in structural conformation, molecular arrangement and surface density of biotin functional groups may affect the subsequent assembly of SA-QDs *via* bio-SA interaction. To determine which factor contributes more (linker length or number density of QDs) to the observed stronger fluorescence from the MMAPA–peptide-linked QD arrays, we combine AFM with fluorescence spectroscopy.

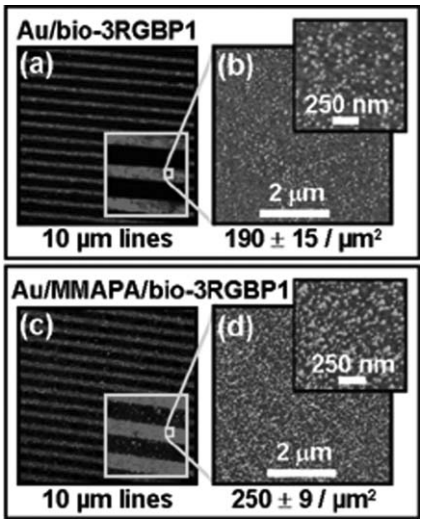

Fig. 3 Peptide-mediated surface-immobilized QD hybrid nanoassemblies. Fluorescence images show precise alignment of the QD arrays, good reproducibility, and uniformity of the peptide-mediated self-assembly of QDs over large areas. Unlike thiol linkers that have a propensity to reactive spreading, peptide linkers enable site-specific self-assembly through surface recognition. (a,b) Emission and the corresponding QD coverage within peptide-linked QD arrays. (c,d) Emission and the corresponding QD coverage within MMAPA–peptide-linked QD arrays. During the backfilling of the OEG-patterned gold substrate with MMAPA, place-exchange reactions between MMAPA and OEG molecules took place. As a result, some non-specific QD attachment is observed (inset of fluorescence image), highlighting a shortcoming of thiol linkers in terms of stable binding to the substrate. However, covalent attachment of peptides onto SAM of MMAPA results in the denser packing of chemically grafted peptide linkers. This results in a greater surface density of biotin functional groups in MMAPA–peptide-linked arrays. This in turn enables more QDs to assemble through a greater number of biotin–streptavidin interactions. The average QD attachment densities are 250 ± 9 μm^{-2} and 190 ± 15 μm^{-2} in MMAPA–peptide-linked arrays and peptide-linked arrays respectively—a difference of ~32% in QD coverage.

AFM characterization showed that the QD coverage in peptide-linked arrays (Fig. 3b) is less than that in MMAPA–peptide-linked arrays (Fig. 3d). This may be attributed to the greater surface density of biotin functional groups, which enables more QDs to assemble (see below for further explanation). To quantify the differences in QD coverage, three samples were prepared with each type of attachment chemistry and five random regions were characterized by AFM for each sample. From AFM measurements, we calculated the average QD attachment density to be 190 ± 15 μm^{-2} (Fig. 3b) and 250 ± 9 μm^{-2} (Fig. 3d) for self-assembled bio-3RGBP1 and MMAPA-grafted bio-3RGBP1 respectively. This corresponds to a ~32% increase in QD coverage within the MMAPA–peptide-linked QD arrays.

As shown in Fig. 4, self-assembled bio-3RGBP1 and MMAPA-grafted bio-3RGBP1 exhibit distinct morphological

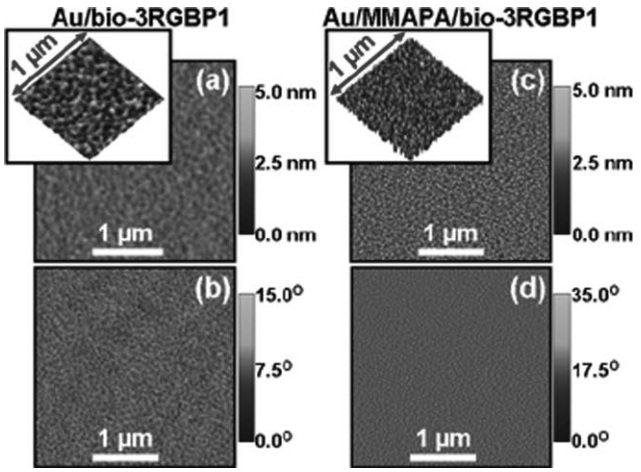

Fig. 4 AFM morphological analysis of peptide linkers and MMAPA-grafted peptide linkers. Height (a, c) and phase (b, d) images were acquired simultaneously. As a result of fundamentally different immobilization mechanisms, self-assembled peptides on gold substrate (a, b) and MMAPA-grafted peptides (c, d) exhibit distinct morphological features. (a, b) Self-assembled bio-3RGBP1 makes an intimate contact with the gold substrate, producing a smooth, uniform, and well-ordered surface. (c, d) Physically constrained by the covalent linkages, MMAPA-grafted bio-3RGBP1 is densely packed and highly oriented. Insets in (a) and (c) are 3-D topographical profiles of self-assembled bio-3RGBP1 and MMAPA-grafted bio-3RGBP1 respectively.

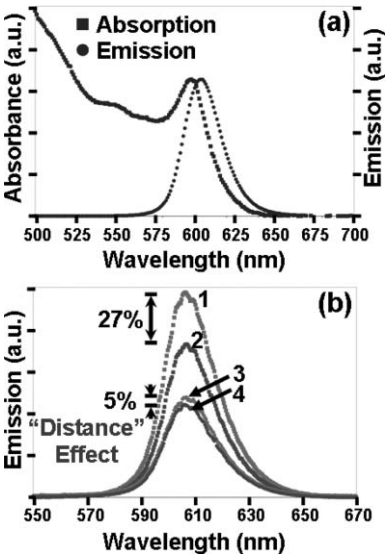

Fig. 5 Photoluminescence measurements. (a) The absorption and emission spectra of SA-QDs in solution. (b) The emission spectra of peptide-mediated surface-immobilized QD hybrid nanoassemblies. Spatially resolved spectral measurements within each 10 μm line enable a quantitative comparison of the PL from QD arrays. The emission intensity from MMAPA–peptide-linked QD arrays (1) was ~27% greater than that from peptide-linked QD arrays (2). After normalization of the emission intensity for each pattern with respect to the average QD attachment density, the fluorescence per dot from peptide–MMAPA-linked QDs (3) is ~5% stronger than that from peptide-linked QDs (4).

features. Due to fundamentally different immobilization mechanisms, the structural conformations of covalently bonded bio-3RGBP1 on the SAM of MMAPA are significantly different from the molecular arrangement (ordering, packing, orientation, and flexibility) of self-assembled bio-3RGBP1 on gold substrates. During immobilization onto the gold substrate, bio-3RGBP1 dynamically repositions itself to maximize its interaction with the gold substrate (*i.e.*, surface recognition) by spreading out to achieve an intimate contact, producing a smooth, uniform, and well-ordered surface (Fig. 4a, b). A topographical 3-D profile (Fig. 4a, inset) shows that the layer of bio-3GBP1 is conformal with the individual grains of the gold surface. In contrast, the surface presented by MMAPA-grafted bio-3RGBP1 is densely packed and more highly oriented (Fig. 4c, d). As evident in the topographical 3-D profile (Fig. 4c, inset), physical constraints imposed by the covalent linkages at periodic intervals on the reactive SAM cause the denser packing of chemically grafted bio-3RGBP1, resulting in a greater surface density of biotin functional groups. This in turn allows more QDs to assemble through a greater number of biotin–streptavidin interactions.

At high solid-state packing densities,[33] the fluorescence peak from a QD film can be red-shifted from that of the QDs in solution due to energy transfer between QDs of different sizes. Spectral characterizations of SA-QDs in solution and peptide-mediated surface-immobilized hybrid QD nanoassemblies organized in arrays of 10 μm lines are given in Fig. 5. The emission maximum from QDs in solution (Fig. 5a) and in the solid state (Fig. 5b) is the same (*i.e.*, near 605 nm), suggesting little inter-dot energy transfer is taking place at the observed surface attachment densities in both arrays. Moreover, there was no noticeable broadening in the emission spectra of surface-immobilized hybrid nanostructures; the FWHM remained unchanged at ~30 nm following the assembly of QDs from solution. This is not surprising, given the relatively narrow size distribution of QDs used, and the fact that their Förster resonance energy transfer radius is ~4–5 nm,[33] and their inorganic shell and ligand coating are ~5.2–6.6 nm thick.[23]

We now return to the question of whether the increased fluorescence observed from the MMAPA–peptide-linked QD arrays arises from longer QD–metal spacing, higher number density of QDs, or both. To compare fluorescence intensities, the samples were illuminated with a 532 nm CW laser at 5.7 W cm^{-2} and the emission spectra were recorded with a 100 ms integration time. Fluorescence intensities were reproducible from region to region within ~3% in both arrays.

Spatially resolved spectral measurements within each 10 μm line enable a quantitative comparison of the PL from QD arrays (Fig. 5b). Consistent with the observation under fluorescence microscopy, the emission intensity from arrays of hybrid nanostructures with MMAPA (1) was ~27% stronger than that from arrays of hybrid nanostructures without MMAPA (2). After normalization of the emission intensity for each pattern with respect to the average QD attachment density (3 and 4), the fluorescence per dot from MMAPA–peptide-linked QDs is ~5% stronger than that from peptide-linked QDs. We thus conclude that while both linker length and number density of QDs affect the luminescence properties of the arrays, the main cause of the difference in

fluorescence intensities is the difference in average QD attachment densities.

Conclusions

In conclusion, we have shown the utility of combinatorially selected peptides in generating periodic arrays of hybrid nanostructures. In view of the potential of combinatorial biology technologies to identify peptides with surface recognition for specific metals, metal oxides, or semiconductor materials, the utility of GEPIs as biomolecular linkers as demonstrated in this study may allow new routes to assemble nanomaterials and form hybrid nanostructures on various substrates with selectivity for the physical or chemical properties of an inorganic surface. In addition, we have shown that synthetic modification of GEPIs (*i.e.*, covalent attachment to non-biological organic compounds) can further increase their range of behavior and possible functionality. This work establishes a framework for investigating the luminescence properties of surface-immobilized hybrid nanostructures where both the QD–metal distance and the surface attachment density can be monitored and controlled. Spectral studies on energy transfer and optical interactions between QDs and *nanopatterned* metal substrates (as opposed to *planar* metal substrates as used in this study) are under way and will be reported in a subsequent publication.

Acknowledgements

This project was supported partially by the Bioinspired Materials and Systems Program through the Air Force Office of Scientific Research (US-AFOSR), UW-DURINT (Defense University Research Initiative on Nanotechnology) through the Army Research Office (US-ARO), and the GEMSEC (Genetically Engineered Materials Science and Engineering Center) through the NSF-MRSEC program. This research was also supported by a DURIP grant FA9550-05-1-0231 from the US-AFOSR. A. K.-Y. Jen thanks the Boeing-Johnson Foundation for its support. A. M. Munro and M. T. Zin acknowledge the Nanotechnology Fellowships from the Center for Nanotechnology at the University of Washington, a member of the National Nanotechnology Infrastructure Network (NNIN) supported by NSF. C. Tamerler and M. Gungormus thank the Turkish State Planning Organization for its support.

References

1 C. M. Niemeyer, *Angew. Chem., Int. Ed.*, 2001, **40**, 4128; E. Dujardin and S. Mann, *Adv. Mater.*, 2002, **14**, 775; N. C. Seeman and A. M. Belcher, *Proc. Natl. Acad. Sci. U. S. A.*, 2002, **99**, 6452.
2 M. Sarikaya, *Proc. Natl. Acad. Sci. U. S. A.*, 1999, **96**, 14183.
3 G. Xu, W. Wang, J. T. Groves and M. H. Hecht, *Proc. Natl. Acad. Sci. U. S. A.*, 2001, **98**, 3652; J. M. Slocik, J. T. Moore and D. W. Wright, *Nano Lett.*, 2002, **2**, 169; M. G. Ryadnov, B. Ceyhan, C. M. Niemeyer and D. N. Woolfson, *J. Am. Chem. Soc.*, 2003, **125**, 9388; A. Verma, H. Nakade, J. M. Simard and V. M. Rotello, *J. Am. Chem. Soc.*, 2004, **126**, 10806; R. Levy, N. T. K. Thanh, R. C. Doty, I. Hussain, R. J. Nichols, D. J. Schiffrin, M. Brust and D. G. Fernig, *J. Am. Chem. Soc.*, 2004, **126**, 10076; M. M. Stevens, N. T. Flynn, C. Wang, D. A. Tirrell and R. Langer, *Adv. Mater.*, 2004, **16**, 915.
4 G. T. Hermanson, *Bioconjugate Techniques*, Academic Press, New York, 1996.
5 A. C. Templeton, W. P. Wuelfing and R. W. Murray, *Acc. Chem. Res.*, 2000, **33**, 27; F. Caruso, *Adv. Mater.*, 2001, **13**, 11; Y. Xia, P. Yang, Y. Sun, Y. Wu, B. Mayers, B. Gates, Y. Yin, F. Kim and H. Yan, *Adv. Mater.*, 2003, **15**, 353; C. Burda, X. Chen, R. Narayanan and M. A. El-Sayed, *Chem. Rev.*, 2005, **105**, 1025.
6 A. P. Alivasatos, *Nat. Biotechnol.*, 2004, **22**, 47; T. Pellegrino, S. Kudera, T. Liedl, A. M. Javier, L. Manna and W. J. Parak, *Small*, 2005, **1**, 48; N. L. Rosi and C. A. Mirkin, *Chem. Rev.*, 2005, **105**, 1547.
7 M. Bruchez, M. Moronne, P. Gin, S. Weiss and A. P. Alivisatos, *Science*, 1998, **281**, 2013; W. C. W. Chan and S. Nie, *Science*, 1998, **281**, 2016.
8 E. R. Goldman, G. P. Anderson, P. T. Tran, H. Mattoussi, P. T. Charles and J. M. Mauro, *Anal. Chem.*, 2002, **74**, 841; I. L. Medintz, A. R. Clapp, H. Mattoussi, E. R. Goldman, B. Fisher and J. M. Mauro, *Nat. Mater.*, 2003, **2**, 630.
9 F. Pinaud, D. King, H.-P. Moore and S. Weiss, *J. Am. Chem. Soc.*, 2004, **126**, 6115.
10 D. M. Willard, L. L. Carillo, J. Jung and A. Van Orden, *Nano Lett.*, 2001, **1**, 469; S. Wang, N. Mamedova, N. A. Kotov, W. Chen and J. Studer, *Nano Lett.*, 2002, **2**, 817; S.-Y. Ding, M. Jones, M. P. Tucker, J. M. Nedeljkovic, J. Wall, M. N. Simon, G. Rumbles and M. E. Himmel, *Nano Lett.*, 2003, **3**, 1581; J. Lee, A. O. Govorov, J. Dulka and N. A. Kotov, *Nano Lett.*, 2004, **4**, 2323.
11 R. A. McMillan, C. D. Paavola, J. Howard, S. L. Chan, N. J. Zaluzec and J. D. Trent, *Nat. Mater.*, 2002, **1**, 247; K. E. Sapsford, I. L. Medintz, J. P. Golden, J. R. Deschamps, H. T. Uyeda and H. Mattoussi, *Langmuir*, 2004, **20**, 7720.
12 Y. Cui, M. T. Björk, J. A. Liddle, C. Sönnichsen, B. Boussert and A. P. Alivisatos, *Nano Lett.*, 2004, **4**, 1093.
13 D. Zhou, A. Bruckbauer, C. Abell, D. Klenerman and D. Kang, *Adv. Mater.*, 2005, **17**, 1243; O. Kulakovich, N. Strekal, A. Yaroshevich, S. Maskevich, S. Gaponenko, I. Nabiev, U. Woggon and M. Artemyev, *Nano Lett.*, 2002, **2**, 1449.
14 K. V. Sarathy, P. J. Thomas, U. Kulkarni and C. N. R. Rao, *J. Phys. Chem. B*, 1999, **103**, 399; Z. Hens, D. V. Tallapin, H. Weller and D. Vanmaekelbergh, *Appl. Phys. Lett.*, 2002, **81**, 4245; J. Tang, H. Birkeldal, E. W. McFaland and G. D. Stucky, *Chem. Commun.*, 2003, 2278.
15 M. Sarikaya, C. Tamerler, A. K.-Y. Jen, K. Schulten and F. Baneyx, *Nat. Mater.*, 2003, **2**, 577; M. Sarikaya, C. Tamerler, D. T. Schwartz and F. Baneyx, *Annu. Rev. Mater. Res.*, 2004, **34**, 373.
16 E. E. Oren, C. Tamerler and M. Sarikaya, *Nano Lett.*, 2005, **5**, 415; C. Tamerler, M. Duman, E. E. Oren, M. Gungormus, X. Xiong, T. Kacar, B. A. Parvis and M. Sarikaya, *Small*, 2006, **2**, 1372.
17 S. Brown, M. Sarikaya and E. Johnson, *J. Mol. Biol.*, 2000, **299**, 725.
18 C. Tamerler, E. E. Oren, M. Duman, E. Ventakasubramanian and M. Sarikaya, *Langmuir*, 2006, **22**, 7712.
19 C. K. Thai, H. X. Dai, M. S. R. Sastry, M. Sarikaya, D. T. Schwartz and F. Baneyx, *Biotechnol. Bioeng.*, 2004, **87**, 129.
20 S. R. Whaley, D. S. English, E. L. Hu, P. F. Barbara and A. M. Belcher, *Nature*, 2000, **405**, 665; K. Goede, P. Busch and M. Grundmann, *Nano Lett.*, 2004, **4**, 2115.
21 S. Brown, *Proc. Natl. Acad. Sci. U. S. A.*, 1992, **89**, 8651; S. Brown, *Nat. Biotechnol.*, 1997, **15**, 269; S. Nygaard, R. Wendelbo and S. Brown, *Adv. Mater.*, 2002, **14**, 1853.
22 P. C. Weber, D. H. Ohlendorf, J. J. Wendoloski and R. R. Salemme, *Science*, 1989, **243**, 85; T. Sano and C. R. Cantor, *J. Biol. Chem.*, 1990, **265**, 3369.
23 E. Oh, M.-Y. Hong, D. Lee, S.-H. Nam, H. C. Yoon and H.-S. Kim, *J. Am. Chem. Soc.*, 2005, **127**, 3270.
24 Y. Xia and G. M. Whitesides, *Annu. Rev. Mater. Sci.*, 1998, **28**, 153; Y. Xia and G. M. Whitesides, *Angew. Chem., Int. Ed.*, 1998, **37**, 550.
25 K. L. Prime and G. M. Whitesides, *Science*, 1991, **252**, 1164; C. Pale-Grosdemange, E. S. Simon, K. L. Prime and G. M. Whitesides, *J. Am. Chem. Soc.*, 1991, **113**, 12; K. L. Prime and G. M. Whitesides, *J. Am. Chem. Soc.*, 1993, **115**, 10714.
26 R. S. Kane, S. Takayama, E. Ostuni, D. E. Ingber and G. M. Whitesides, *Biomaterials*, 1999, **20**, 2363; M. Mrksich, *Curr. Opin. Chem. Biol.*, 2002, **6**, 794.

27 L. Yan, X. Zhao and G. M. Whitesides, *J. Am. Chem. Soc.*, 1998, **120**, 6179; G. H. Degenhart, B. Dordi, H. Schonherr and G. J. Vancso, *Langmuir*, 2004, **20**, 6216.
28 R. C. Horton, Jr., T. M. Herne and D. C. Myles, *J. Am. Chem. Soc.*, 1997, **119**, 12980.
29 M. T. Zin, H. Ma, M. Sarikaya and A. K.-Y. Jen, *Small*, 2005, **1**, 698.
30 M. T. Zin, H.-L. Yip, N.-Y. Wong, H. Ma and A. K.-Y. Jen, *Langmuir*, 2006, **22**, 6346.
31 K. T. Shimizu, W. K. Woo, B. R. Fisher, H. J. Eisler and M. G. Bawendi, *Phys. Rev. Lett.*, 2002, **89**, 117401.
32 W. L. Barnes, *J. Mod. Opt.*, 1998, **45**, 661.
33 C. R. Kagan, C. B. Murray and M. G. Bawendi, *Phys. Rev. B*, 1996, **54**, 8633.

